

Exploring the tim elike region for the elastic form factors in a scalar eld theory

Ho-M eoyng Choi and Chueng-R yong Ji

Department of Physics, North Carolina State University, Raleigh, N.C. 27695-8202

We investigate the form factors of $q\bar{q}$ bound states both in spacelike and tim elike region using an exactly solvable model of $(3+1)$ dimensional scalar eld theory interacting with gauge elds. Based on the light-front quantization, the Drell-Yan-West ($q^+ = 0$) frame as well as the purely longitudinal momentum ($q^+ \neq 0$ and $q_z = 0$) frame were used for the calculations of the form factors of $M \rightarrow \pi + M$ transitions. We then analytically continue the form factors in the spacelike region to the tim elike region and compare those with the direct results of the tim elike form factors of $\pi \rightarrow M + M$ transitions. Our results verify the exact equivalence of the two results and exhibit that the method of analytic continuation automatically yields the effect of complicated nonvalence contributions. The meson peaks analogous to the vector meson dominance (VMD) phenomena are also generated at the usual VMD positions.

I. INTRODUCTION

The Drell-Yan-West ($q^+ = q^0 + q^3 = 0$) frame in the light-front quantization provided an effective formulation for the calculation of various form factors in the space-like momentum transfer region $q^2 = -Q^2 < 0$ [1]. In $q^+ = 0$ frame, only parton-number-conserving Fock state (valence) contribution is needed when the "good" components of the current, j^+ and $j_- = (j_x; j_y)$, are used [2]. For example, only the valence diagram shown in Fig. 1 (a) is used in the light-front quark model analysis of spacelike meson form factors. Successful light-front quark model description of various hadron form factors can be found in the literatures [3-6].

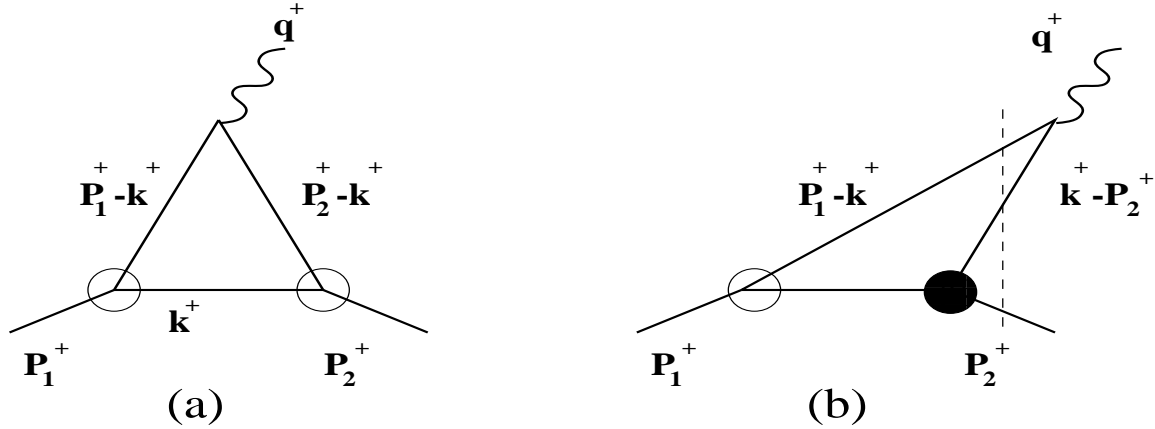


FIG. 1. The light-front quark model description of an electroweak meson form factor: (a) the usual light-front valence diagram and (b) the nonvalence (pair-creation) diagram. The vertical dashed line in (b) indicates the energy-denominator for the nonvalence contributions. While the white blob represents the usual light-front valence wave function, the modeling of black blob has not yet been made.

However, the timelike ($q^2 > 0$) form factor analysis in the light-front quark model has been hindered by the fact that $q^+ = 0$ frame is defined only in the spacelike region ($q^2 = q^+ q^- - \mathbf{q}_\perp^2 < 0$). While the $q^+ \neq 0$ frame can be used in principle to compute the timelike form factors, it is inevitable in this frame to encounter the nonvalence diagram arising from the quark-antiquark pair creation (so called "Z-graph"). For example, the nonvalence diagram in the case of semileptonic meson decays is shown in Fig. 1 (b). The main source of the difficulty, however, in calculating the nonvalence diagram (see Fig. 1 (b)) is the lack

of information on the black blob which should contrast with the white blob representing the usual light-front valence wave function. In fact, it was reported [2] that the omission of nonvalence contribution leads to a large deviation from the full results. The timelike form factors associated with the hadron pair productions in e^+e^- annihilations also involve the nonvalence contributions. Therefore, it would be very useful to avoid encountering the nonvalence diagram and still be able to generate the results of timelike form factors.

In this paper, we show an explicit example of generating the exact result of the timelike form factor without encountering the nonvalence diagram. This can be done by the analytic continuation from the spacelike form factor calculated in the Drell-Yan-West ($q^+ = 0$) frame to the timelike region. To explicitly show it, we use an exactly solvable model of $(3+1)$ dimensional scalar field theory interacting with gauge fields. In this model, we calculate: (A) the timelike process of $\pi^0 \rightarrow M^+ M^-$ transition in $q^+ \neq 0$ ($q^2 > 0$) frame, (B) the spacelike process of $M^0 \rightarrow M^+ M^-$ in $q^+ \neq 0$ ($q^2 < 0$) frame, and (C) the spacelike process of $M^0 \rightarrow M^+ M^-$ in $q^+ = 0$ frame. Using the analytic continuation from $q^2 < 0$ to $q^2 > 0$, we show that the result in (C), which is obtained without encountering the nonvalence contributions at all, exactly reproduces the result in (A). In fact, all three results (A), (B), and (C) coincide with each other in the entire q^2 range. We also confirm that our results are consistent with the dispersion relations [7,10]. We consider not only for the equal quark and antiquark case such as the pion but also for the unequal meson productions such as K and D .

The paper is organized as follows: In Sec. II, we derive the timelike electromagnetic (EM) form factor of $\pi^0 \rightarrow M^+ M^-$ process in the $q^+ \neq 0$ frame (A) and discuss the singularities occurring from the on-energy shell of quark-antiquark pair creation. In Sec. III, the spacelike form factor of $M^0 \rightarrow M^+ M^-$ process is calculated both in the $q^+ \neq 0$ (B) and $q^+ = 0$ frames (C). We then analytically continue the spacelike form factors to the timelike region. The singularities occurred in the timelike region are also discussed. In Sec. IV, we numerically calculate the EM form factors of the π , K , and D mesons for three different cases (A), (B), and (C) using our constituent quark and antiquark masses ($m_u = m_d = 0.25$ GeV, $m_s = 0.48$ GeV, and $m_c = 1.8$ GeV) [6,2,11] and show that the form factors obtained from

those three different cases are equal to each other for the entire q^2 region. The meson peaks analogous to the vector meson dominance (VMD) are also discussed. The conclusion and discussion follows in Sec. V.

II. FORM FACTORS IN THE TIMELIKE REGION

The electromagnetic (EM) local current $J(0)$ responsible for a virtual photon decay into two $q\bar{Q}$ bound states in the scalar field theory can be calculated using the diagrams shown in Fig. 2. The covariant diagram shown in Fig. 2 (a) is equivalent to the sum of two light-front time-ordered diagrams in Figs. 2 (b) and 2 (c). The EM current $J(0)$ obtained from the covariant diagram of Fig. 2 (a) is given by

$$J(0) = e_q \int \frac{d^4k}{(2\pi)^4} \frac{1}{(q-k)^2 - m_q^2 + i} (q-2k) \frac{1}{(q-k-P_2)^2 - m_Q^2 + i} \frac{1}{k^2 - m_q^2 + i} + e_Q (\text{m}_q \leftrightarrow \text{m}_Q \text{ of the 1st term}); \quad (1)$$

where $m_{q(Q)}$ and $e_{q(Q)}$ are the constituent quark (antiquark) mass and charge, respectively. The corresponding form factor of the $q\bar{Q}$ bound state in timelike ($q^2 > 0$) region is defined by

$$J(0) = (P_1 - P_2) F(q^2); \quad (2)$$

where $q = P_1 + P_2$, $P_1^2 = P_2^2 = M^2$ and M is the mass of a $q\bar{Q}$ bound state scalar particle.

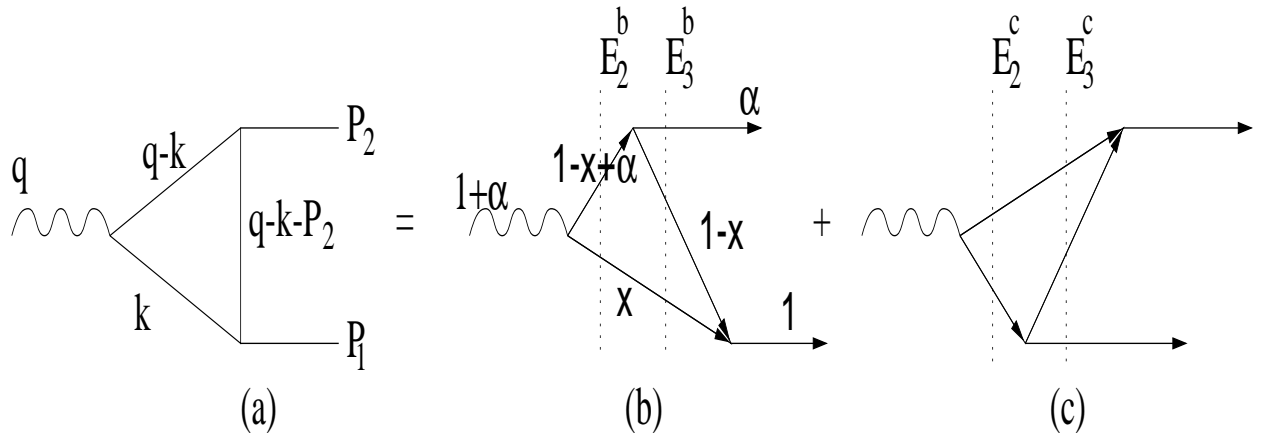


FIG. 2. The electromagnetic decays of a photon into two-body bound states, i.e., $1 \rightarrow q\bar{q}$ (or $Q\bar{Q}$) $\rightarrow M(q\bar{Q})M(\bar{q}Q)$, in scalar theory: Covariant representation (a), and the light-front time ordered contributions to the decay amplitude (b) and (c).

Using the Cauchy integration over k^- in Eq. (1), we can find each time-ordered contribution (Figs. 2(b) and 2(c)) to the timelike form factor $F(q^2 > 4M^2)$ in Eq. (2). This procedure allows us to analyze the singularity structure of each light-front time-ordered diagram as well. For the calculation of each light-front time-ordered contribution, we take the purely longitudinal momentum frame, i.e., $q_1^+ \neq 0$, $q_2^- = 0$ and $P_{1?} = P_{2?} = 0$. Accordingly, $q^2 (= q_1^+ q_1^-) > 4M^2$ is given by

$$q^2 = M^2(1 + \beta)^2; \quad (3)$$

where $\beta = P_2^+ = P_1^+ = q_1^+ = P_1^+ - 1$ is the longitudinal momentum fraction and the two solutions for β are given by

$$\beta = \frac{q^2}{2M^2} - 1 \pm \sqrt{\left(\frac{q^2}{2M^2} - 1\right)^2 - 1}; \quad (4)$$

Note that both $\beta = 1$ correspond to the threshold, $q^2 = 4M^2$. The EM form factor $F(q^2)$ in Eq. (2) is independent of the subscript sign of β . Thus, one can take either β_+ or β_- to calculate $F(q^2)$. Here, we use, for convenience, $\beta = \beta_+$, which ranges from 0 to 1 for the physical momentum transfer region, i.e., $0 \leq q^2 \leq 1$ and $1 \leq q^2 \leq 4M^2$. Of course, we can use $\beta = \beta_-$ equally well and verify that the two results (β_+ and β_-) are exactly same for the calculation of $F(q^2)$.

Since $q_1^+ > P_1^+ - P_2^+ > 0$ for $\beta = \beta_+$, the Cauchy integration over k^- in Eq. (1) has two nonzero contributions to the residue calculations, one coming from the interval (i) $0 < k^+ < P_1^+$ (see Fig. 2(b)) and the other from (ii) $P_1^+ < k^+ < q_1^+$ (see Fig. 2(c)). The internal momentum k^+ is defined by $k^+ = xP_1^+$, where x is the Lorentz invariant longitudinal momentum variable. The "good"-current $J^+(0)$ is used in our computation of the two light-front diagrams Figs. 2(b) and 2(c). In the following, for simplicity, we won't explicitly write either the obvious second term in Eq. (1) nor the charge factor (e_q or $e_{\bar{q}}$).

In the region of $0 < k^+ < P_1^+$, the residue is at the pole of $k^- = [m_q^2 + k_\perp^2 - i]k^+$, which is placed in the lower half of complex- k plane. Thus, the Cauchy integration of J^+ in Eq. (1) over k^- in this region gives

$$J_b^+(0) = N \int_0^{P_1^+} dk^+ \int d^2k_\perp \frac{q^+ - 2k^+}{k^+ (q^+ - k^+) (P_1^+ - k^+)} \frac{1}{q^+ - (m_q^2 + k_\perp^2) = k^+ - (m_q^2 + k_\perp^2) = (q^+ - k^+)} \frac{1}{q^+ - P_2 - (m_q^2 + k_\perp^2) = k^+ - (m_q^2 + k_\perp^2) = (P_1^+ - k^+)}; \quad (5)$$

where the subscript b in $J_b^+(0)$ implies the current in Fig. 2(b) and N ($= i$) is the normalization constant. The second and third terms in Eq. (5) correspond to the two particle, i.e., the forward propagator of the particle and antiparticle produced by the incoming photon, and the three particle intermediate states, respectively. We represent the energy denominators of the two and three particle states as E_2^b and E_3^b in Fig. 2(b), respectively.

To analyze the singularities of Eq. (5), we further integrate over k_\perp and obtain

$$J_b^+(0) = N \int_0^{P_1^+} dx \frac{x(1+x) = (1+x)}{E_3^b - E_2^b} \ln \frac{E_2^b}{E_3^b}; \quad (6)$$

where $E_2^b = x(1+x)M^2 = m_q^2$ and $E_3^b = x(1+x)M^2 - [xm_q^2 + (1-x)m_Q^2]$. While E_3^b is not zero ($E_3^b \neq 0$) in general for the entire physical region, E_2^b can be zero when $q^2 = 4m_{q(Q)}^2$. The singular structure of $E_3^b - E_2^b$ term in Eq. (6) depends on whether a qQ bound state scalar particle is strongly bounded ($M^2 < m_q^2 + m_Q^2$) or weakly bounded ($M^2 > m_q^2 + m_Q^2$). As we will show in our numerical calculations (Section IV), anomalous singularities appear for $M^2 > m_q^2 + m_Q^2$ while only the normal threshold of bound state exists for $M^2 < m_q^2 + m_Q^2$.

In the region of $P_1^+ < k^+ < q^+$, the residue is at the pole of $k^- = q^+ - [m_q^2 + (q_\perp^2 - k_\perp^2)^2]k^+$, which is placed in the upper half of complex- k plane. Thus, the Cauchy integration of $J^+(0)$ in Eq. (1) over k^- in this region yields the result

$$J_c^+(0) = N \int_{P_1^+}^{q^+} dk^+ \int d^2k_\perp \frac{q^+ - 2k^+}{k^+ (q^+ - k^+) (P_1^+ - k^+)} \frac{1}{q^+ - (m_q^2 + k_\perp^2) = k^+ - (m_q^2 + k_\perp^2) = (q^+ - k^+)} \frac{1}{q^+ - P_1 - (m_q^2 + k_\perp^2) = (q^+ - k^+)};$$

$$\frac{1}{q^2 - P_1^2 + (m_Q^2 + k_2^2) = (P_1^+ - k^+)(m_Q^2 + k_2^2) = (q^+ - k^+)}; \quad (7)$$

where the subscript c in $J_c^+(0)$ implies the current in Fig. 2(c). After the integration over the k_2 in Eq. (7), we obtain

$$J_c^+(0) = \frac{N}{2} \int_0^1 dx \frac{x(1+2x)}{E_3^c - E_2^c} \ln \frac{E_2^c}{E_3^c}; \quad (8)$$

where $x = 1 + (1 - X)$, $E_3^c = X(1 - X)M^2 - [m_Q^2 + (1 - X)m_q^2]$ and $E_2^c = X(1 + X)M^2 - m_q^2$. The pole structure in Eq. (8) is equivalent to that of Eq. (6).

Consequently, the timelike form factor in Eq. (2) is given by

$$F(q^2) = \frac{N}{2} \int_0^1 dx \frac{x(1+2x)}{E_3^b - E_2^b} \ln \frac{E_2^b}{E_3^b} - \frac{x(1+2x)}{E_3^c - E_2^c} \ln \frac{E_2^c}{E_3^c}; \quad (9)$$

where E_2^b, E_3^b, E_2^c and E_3^c are defined in Eqs. (6) and (8).

III. FORM FACTORS IN SPACELIKE REGION AND THE ANALYTIC CONTINUATION TO THE TIMELIKE REGION

In this section, we calculate the EM form factor in spacelike momentum transfer region. We then analytically continue to the timelike region and compare the result with the timelike form factor (i.e. Eq. (9)) that we obtained in the previous section.

The EM current of a qQ bound state in spacelike momentum transfer region is defined by the local current $j(0)$;

$$j(0) = (P_1 + P_2) F(q^2); \quad (10)$$

where $q = P_1 - P_2$ and $q^2 < 0$.

The EM current $j(0)$ obtained from the covariant triangle diagram of Fig. 3(a) is given by

$$j(0) = \int d^4k \frac{1}{(P_1 - k)^2 - m_q^2 + i} (P_1 + P_2 - 2k) \frac{1}{(P_2 - k)^2 - m_q^2 + i} \frac{1}{k^2 - m_Q^2 + i}; \quad (11)$$

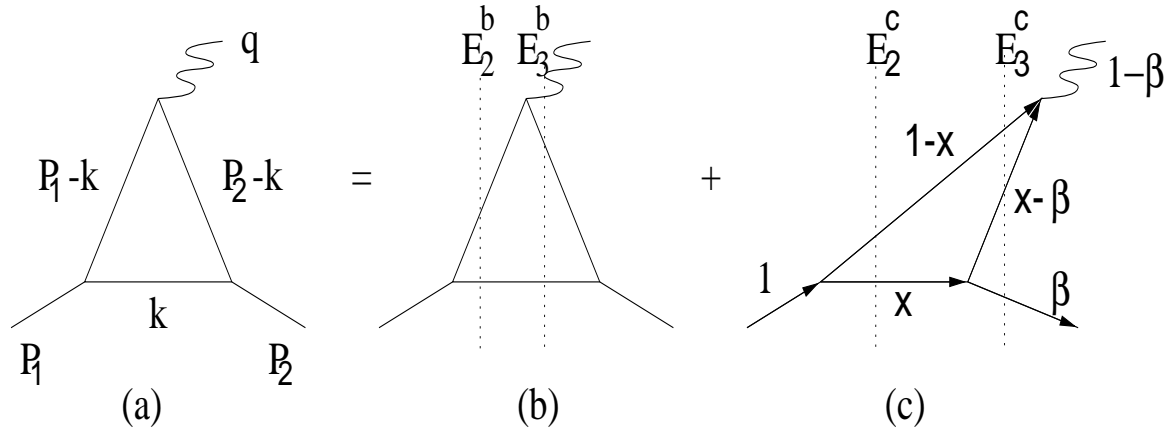


FIG. 3. Covariant triangle diagram (a) is represented as the sum of light-front triangle diagram (b) and the light-front pair-creation diagram (c).

As in the case of the timelike form factor in Sec. II, the Cauchy integration of k in Eq. (11) has also two contributions to the residue calculations, one coming from the interval $0 < k^+ < P_2^+$ (see Fig. 3(b)) and the other from $P_2^+ < k^+ < P_1^+$ (see Fig. 3(c)). Again, only the "good" current $j^+(0)$ in Eq. (11) is used to obtain the contributions from Figs. 3(b) and 3(c).

In the region of $0 < k^+ < P_2^+$, the residue is at the pole of $k = \sqrt{m_q^2 + k_\perp^2} - i\epsilon k^+$, which is placed in the lower half of complex- k plane. Thus, the Cauchy integration of j^+ in Eq. (11) over k in this region yields

$$j_b^+(0) = N \int_0^{P_2^+} dk^+ d^2 k_\perp \frac{(P_1 + P_2 - 2k)^+}{(P_1 - k)^+ (P_1 - k - q)^+ k^+} \frac{1}{\sqrt{P_1 - q} \sqrt{m_q^2 + k_\perp^2} \sqrt{(P_1^+ - k^+) \sqrt{m_q^2 + k_\perp^2} \sqrt{k^+}}} \frac{1}{P_1 - q \sqrt{m_q^2 + (k_\perp + q_\perp)^2} \sqrt{(P_1^+ - k^+) \sqrt{m_q^2 + k_\perp^2} \sqrt{k^+}}}; \quad (12)$$

where the subscript b in $j_b^+(0)$ implies the current in Fig. 3(b).

In the region of $P_2^+ < k^+ < P_1^+$, the residue is at the pole of $k = P_1 - \sqrt{m_q^2 + k_\perp^2} - i\epsilon (P_1^+ - k^+)$, which is placed in the upper half of complex- k plane. Thus, the Cauchy integration of j^+ in Eq. (11) over k in this region becomes

$$j_c^+(0) = N \int_{P_2^+}^{P_1^+} dk^+ d^2 k_\perp \frac{(P_1 + P_2 - 2k)^+}{(P_1 - k)^+ (P_1 - k - q)^+ k^+}$$

$$\begin{array}{c}
1 \\
\hline
P_1 \quad [m_q^2 + k_z^2] = (P_1^+ - k^+) \quad [m_Q^2 + k_z^2] = k^+ \\
\hline
1 \\
\hline
P_2 \quad P_1 + [m_q^2 + k_z^2] = (P_1^+ - k^+) \quad [m_q^2 + (q_z + k_z)^2] = (P_2^+ - k^+)
\end{array} : \quad (13)$$

As one can see from Eq. (13), the nonvalence contribution (Fig. 3(c)) vanishes only in $q^+ = 0$ frame. In the following, we investigate the spacelike form factor $F(q^2)$ given in Eq. (10) using both $q^+ \neq 0$ and $q^+ = 0$ frames. We then analytically continue to the timelike region in order to compare the result with the direct calculation of the timelike form factor $F(q^2)$ presented in the previous section.

A. The $q^+ \neq 0$ and $q_z = 0$ frame

In the purely longitudinal momentum frame $q^+ \neq 0$, $q_z = 0$, and $P_{1z} = P_{2z} = 0$, the momentum transfer $q^2 = q^+ q_-$ can be written in terms of the longitudinal momentum fraction $x = P_2^+ / P_1^+ = 1 - q^+ / P_1^+$;

$$q^2 = -M^2(1-x)^2 = 0; \quad (14)$$

where the two solutions of q^2 are given by

$$x = 1 \pm \frac{q^2}{2M^2} \pm \sqrt{1 - \frac{q^2}{2M^2}} : \quad (15)$$

The form factor $F(q^2)$ in Eq. (10) is also independent of the subscript sign of q . However, $P_2^+ - P_1^+$ was used in obtaining Eqs. (12) and (13) and thus here we use $q^+ = 0$

1) in spacelike region. As shown in Eqs. (11)–(13), the sum of valence (Fig. 3(b)) and nonvalence (Fig. 3(c)) diagrams is equivalent to the covariant triangle diagram in Fig. 3(a).

For the analysis of singularity structures, we integrate over k_z and obtain from the valence contribution (Fig. 3(b));

$$j_b^+(0) = N \int_0^1 dx \frac{x(1-x)}{E_3^b E_2^b} \ln \frac{E_2^b}{E_3^b}; \quad (16)$$

where $E_3^b = x(1-x)M^2 - [xm_q^2 + (1-x)m_Q^2]$ and $E_2^b = x(1-x)M^2 - [xm_q^2 + (1-x)m_Q^2]$. It turns out that Eq. (16) has no singularities because $E_3^b \notin 0$, $E_2^b \notin 0$, and $E_3^b - E_2^b \notin 0$ for the entire q^2 region. On the other hand, the k_z integration for the current $j_c^+(0)$ in Eq. (13) yields

$$j_c^+(0) = N \int_0^1 dx \frac{(1-x)^2 x (2x-1)}{E_2^c - E_3^c} \ln \frac{E_3^c}{E_2^c}; \quad (17)$$

where $x = 1 - (1-x)X$, $E_3^c = (1-x)X [1 - (1-x)X] M^2 - [(1-x)X m_Q^2 + (1 - (1-x)X) m_q^2]$ and $E_2^c = (1-x)^2 X (1-X) M^2 - m_q^2$. While the energy denominator E_2^c of the two particle intermediate state does not vanish both in spacelike and timelike region, the E_3^c of the three particle intermediate state is not zero only for the spacelike momentum transfer region. For the timelike region, E_3^c can be zero so that the singularities start at $q_{min}^2 = 4m_{q(Q)}^2$ for $qq(QQ)$ vertex. The singularity structure of $E_2^c - E_3^c$ in Eq. (17) follows the condition of a qQ bound state as presented in the case of timelike form factor calculations of the previous section.

The EM form factor $F(q^2)$ in Eq. (10) of a qQ bound state in $q^+ \notin 0$ frame is then obtained by

$$F(q^2; q^+ \notin 0) = \frac{N}{1 +} \int_0^1 dx \frac{x(1 + \frac{2-x}{E_3^b - E_2^b})}{E_3^b - E_2^b} \ln \frac{E_2^b}{E_3^b} + \frac{(1-x)^2 x (2x-1)}{E_2^c - E_3^c} \ln \frac{E_3^c}{E_2^c}; \quad (18)$$

where q^2 is timelike(space)like for positive(negative) q^2 . According to the analytic continuation, the sign of q^2 in Eq. (18) must be changed from $-$ to $+$ for the timelike region.

B. The Drell-Yan-West ($q^+ = 0$) frame

In Drell-Yan-West frame, $q^+ = 0$, $q^2 = -q_\perp^2$, and $P_{1z} = P_{2z} = 0$, the Ψ' component of the current has only the valence contribution, i.e., $j_b^+(0)$ in Eq. (12). The current $j_b^+(0)$ in $q^+ = 0$ frame is given by

$$j_b^+(0) = N \int_0^1 dx d^2 \vec{x} \frac{2x(1-x)}{(A - \frac{q_\perp^2}{2})^2 - 4x^2 \frac{q_\perp^2}{2} \cos^2 \theta}; \quad (19)$$

where $\gamma = k_z + xq_z = 2$, $A = x(1-x)M^2 - [xm_q^2 + (1-x)m_Q^2]$, and $\beta^2 = x^2q_z^2 = 4$. The angle $(0 \leq \theta \leq \pi)$ is defined by $\gamma = j_z, j_q, j_Q \cos \theta$.

Integrating Eq. (19) over θ and γ , we obtain

$$j_b^+(0) = \int_0^1 dx \int_{-\sqrt{4M^2 + q_z^2}}^{\sqrt{4M^2 + q_z^2}} d\gamma \frac{(1-x)}{(x-x_+)(x-x_-)} \tanh^{-1} \frac{\sqrt{q_z^2}}{4M^2 + q_z^2} \frac{x}{(x-x_+)(x-x_-)}; \quad (20)$$

where

$$x_{\pm} = \frac{2(M^2 - m_q^2 + m_Q^2)}{4M^2 + q_z^2} \pm \frac{\sqrt{4(M^2 - m_q^2 + m_Q^2)^2 - 4m_Q^2}}{(4M^2 + q_z^2)^2}; \quad (21)$$

Our analytic continuation method in the $q^+ = 0$ frame is to change q_z to iq_z in Eqs. (20) and (21) from spacelike to timelike region. We note from Eqs. (20) and (21) that the result of the timelike region exhibits the same singularity structure as the direct analyses in $q^+ \neq 0$ frame, i.e., Eqs. (6) and (17), even though the nonvalence contribution in Fig. 3(c) is absent here.

After some manipulation, we obtain the EM form factor of a qQ bound state in the $q^+ = 0$ frame as follows

$$F(q^2; q^+ = 0) = \int_0^1 ds \frac{4N}{q^2(q^2 - 4M^2)} \frac{\arcsin(\frac{1-a}{b})}{\arcsin(\frac{a}{b})} d(1-a-b\sin\theta) \tanh^{-1} \frac{q^2}{q^2 - 4M^2} \frac{a + b\sin\theta}{ib\cos\theta}; \quad (22)$$

where $a = (x_+ + x_-) = 2$, $b = (x_+ - x_-) = 2$, and $q^2 = -q_z^2$ is time(space)like for positive (negative) q_z^2 . While the representations in Eqs. (18) and (22) look apparently different, it is amazing to realize that the two formulas (Eqs. (18) and (22)) are actually identical as we will show explicitly in the next section of numerical calculations.

IV. NUMERICAL RESULTS

For our numerical analysis of ρ , K , and D meson form factors, we use the physical meson masses together with the following constituent quark and antiquark masses: $m_u = m_d = 0.25$

GeV, $m_s = 0.48$ GeV, and $m_c = 1.8$ GeV [2,6,11]. Since our numerical results of the EM form factors obtained from Eqs. (9), (18), and (22) turn out to be exactly same with each other for the entire q^2 region, only a single line is depicted in Figs. 4, 5 and 6 for the form factor calculations of π , K , and D mesons, respectively.

It should be noted from our constituent masses that $M^2 < m_q^2 + m_Q^2$ for π and K and $M^2 > m_q^2 + m_Q^2$ for D meson cases. As discussed in Ref. [8] for the analysis of the one-particle matrix element of a scalar current, while the singularity for $M^2 < m_q^2 + m_Q^2$ case starts on the positive q^2 -axis at the threshold point $q_{\text{min}}^2 = 4m_{q(Q)}^2$ for $qq(QQ)$ vertex, the singularity for $M^2 > m_q^2 + m_Q^2$ starts at

$$q_{\text{min}}^2 = \frac{1}{m_{Q(q)}^2} [m_{q(Q)}^2 - (M - m_{Q(q)})^2][(M + m_{Q(q)})^2 - m_{q(Q)}^2]; \quad (23)$$

for $qq(QQ)$ vertex. Our numerical results exhibit all of these singular properties coming from the normal (π , K) and anomalous (D) cases. As a consistency check, we shall also compare our numerical results of the form factor $F(q^2) = \text{Re} F(q^2) + i \text{Im} F(q^2)$ with the dispersion relations given by

$$\text{Re} F(q^2) = \frac{1}{-P} \int_{-1}^{+1} \frac{\text{Im} F(q'^2)}{q'^2 - q^2} dq'^2; \quad (24)$$

$$\text{Im} F(q^2) = \frac{1}{-P} \int_{-1}^{+1} \frac{\text{Re} F(q'^2)}{q'^2 - q^2} dq'^2; \quad (25)$$

where P indicates the Cauchy principal value.

In Fig. 4(a), we show the EM form factor of the pion for $2 \text{ GeV}^2 \leq q^2 \leq 3 \text{ GeV}^2$. The imaginary part (the dotted line) of the form factor starts at a single $q_{\text{min}}^2 = 4m_{u(d)}^2 = 0.25 \text{ GeV}^2$, which is consistent with the condition for $M^2 < m_q^2 + m_Q^2$ case. It is interesting to note that the square of the total form factor $|F(q^2)|^2$ (thick solid line) produces a meson-type peak near $q^2 = M^2$. In fact, the peak moves to the right (left) as $m_u = m_d$ increases (decreases). However, it is not yet clear if this model indeed reproduces all the features of the vector meson dominance (VMD) phenomena. Even though the generated position of peak is consistent with VMD, the final state interaction is not included in this simple model calculation. We believe that much more complex mechanisms may be necessary to

reproduce the realistic VMD phenomena. More detailed analysis along this line is under consideration. Nevertheless, it is remarkable that this simple model is capable of generating the peaks and the position of peaks are quite consistent with the VMD.

In Fig. 4(b), we show the timelike form factor of the pion for the entire $q^2 > 0$ region and compare the imaginary part of our direct calculations (dotted line) obtained from Eqs. (9), (18), and (22) with the result (data of black dots) obtained from the dispersion relations given by Eq. (25). Our direct calculation is in an excellent agreement with the solution of the dispersion relations. Our result for the real part are also confirmed to be in complete agreement with the dispersion relations. For high q^2 region, the imaginary part of the form factor is dominant over the real part (thin solid line).

In Fig. 5(a), we show the kaon form factor for $2 \text{ GeV}^2 \leq q^2 \leq 5 \text{ GeV}^2$. The kaon also has normal singularity. However, it has two thresholds for the imaginary parts; one is $q_{\text{in}}^2 = 4m_u^2$ and the other is $q_{\text{in}}^2 = 4m_s^2$. These lead to the humped shape (dotted line) of the imaginary part shown in Fig. 5(a). While we have in principle two vector meson-type pole peaks (i.e. ρ and ω), one can see in Fig. 5(a) only ρ meson-type peak for the timelike kaon EM form factor above the physical threshold at $q_{\text{in}}^2 = 4M_K^2$. We also show in Fig. 5(b) the imaginary part from our direct calculation is in an excellent agreement with that (data of black dots) from the dispersion relations for the entire timelike q^2 region. Again, the imaginary part is predominant for high q^2 region.

In Fig. 6, we show the D meson form factor for $10 \text{ GeV}^2 \leq q^2 \leq 30 \text{ GeV}^2$. Unlike the normal threshold of ρ and K form factor calculations, the D meson form factor shows anomalous singularities according to Eq. (23), i.e., $q_{\text{in}}^2 = 0.24 \text{ GeV}^2$ (compared to $4m_d^2 = 0.25 \text{ GeV}^2$ for normal case) and $q_{\text{in}}^2 = 12.4 \text{ GeV}^2$ (compared to $4m_c^2 = 12.96 \text{ GeV}^2$ for normal case) for the d and c vertices, respectively. Similar to the kaon case in Fig. 5, we also have two unphysical peaks, i.e., ρ and J/ψ (1S) meson type peaks due to d and c quarks, respectively. Nevertheless, the timelike form factor of D meson has no pole structure for the physical $q^2 \geq 4M_D^2$ region. In all of these figures (Figs. 4-6), it is amazing to realize that the numerical result of Eq. (22) obtained from $q^+ = 0$ frame

without encountering the nonvalence diagram coincides exactly with the numerical results of Eqs. (9) and (18) obtained from $q^+ \neq 0$ frame once the analytic continuation is utilized.

V. CONCLUSION AND DISCUSSION

In this work, we investigated the EM form factors of various mesons both in spacelike and timelike region using an exactly solvable model of $(3+1)$ dimensional scalar field theory interacting with gauge fields. Our calculations demonstrated that one can compute the timelike form factor without encountering the nonvalence contributions. We calculated the form factor in spacelike region using the Drell-Yan-West ($q^+ = 0$) frame and showed that its analytic continuation to the timelike region reproduces exactly the direct result of timelike form factor obtained in the longitudinal momentum ($q^+ \neq 0$ and $q_z = 0$) frame. It is remarkable that the analytic continuation of the result in Drell-Yan-West frame to the timelike region automatically generate the effect of the nonvalence contributions to the timelike form factor. Another remarkable result in our model calculations is that the peaks analogous to the VMD were generated and the position of peaks were indeed quite consistent with the VMD. Even though much more detailed analyses including the final state would be necessary to reproduce the entire feature of VMD, our results seem pretty encouraging for further investigations. Using the dispersion relations, we have also confirmed that our numerical results of imaginary parts start at $q_{\text{min}}^2 = 4m_{q(Q)}^2$ and the normal thresholds appear for π and K ($M^2 < m_q^2 + m_Q^2$) systems while the anomalous threshold exists for D ($M^2 > m_q^2 + m_Q^2$) system. Thus, it is hopeful that one can use the same technique of analytic continuation and calculate the timelike form factors in more realistic model. Detailed analysis along this line is underway. Applications to the semileptonic decay processes in $(3+1)$ dimensional scalar field model are also in progress.

We would like to thank G.H. Kim for assisting the numerical analysis of dispersion relations. This work was supported by the U.S. DOE under contracts DE-FG02-96ER40947. The North Carolina Supercomputing Center and the National Energy Research Scientific

Computer Center are also acknowledged for the grant of supercomputer time.

- [1] G. P. Lepage and S. J. Brodsky, Phys. Rev. D 22, 2157 (1980).
- [2] H. M. Choi and C. R. Ji, Phys. Rev. D 59, 034001 (1999).
- [3] P. L. Chung, F. Coester, and W. N. Polyzou, Phys. Lett. B 205, 545 (1988).
- [4] W. Jaus, Phys. Rev. D 44, 2851 (1991).
- [5] F. Cardarelli et al., Phys. Lett. B 332, 1 (1994); Phys. Rev. D 53, 6682 (1996).
- [6] H. M. Choi and C. R. Ji, Phys. Rev. D 59, 074015 (1999); 56, 6010 (1997).
- [7] J. D. Bjorken and S. D. Drell, Relativistic Quantum Fields (McGraw-Hill, New York, 1965), pp. 209-282.
- [8] S. Gasiorowicz, Elementary Particle Physics (Wiley, New York, 1966), pp. 348-362.
- [9] S. Mandelstam, Phys. Rev. Lett. 4, 84 (1960).
- [10] M. Gell-Mann, M. L. Goldberger, and W. Thirring, Phys. Rev. 95, 1612 (1954); M. Goldberger, Phys. Rev. 99, 979 (1955).
- [11] H. M. Choi and C. R. Ji, "Light-Front Quark Model Analysis of Exclusive $0^{-+} \rightarrow 0^{-+}$ Semileptonic Heavy Meson Decays", hep-ph/9903496.

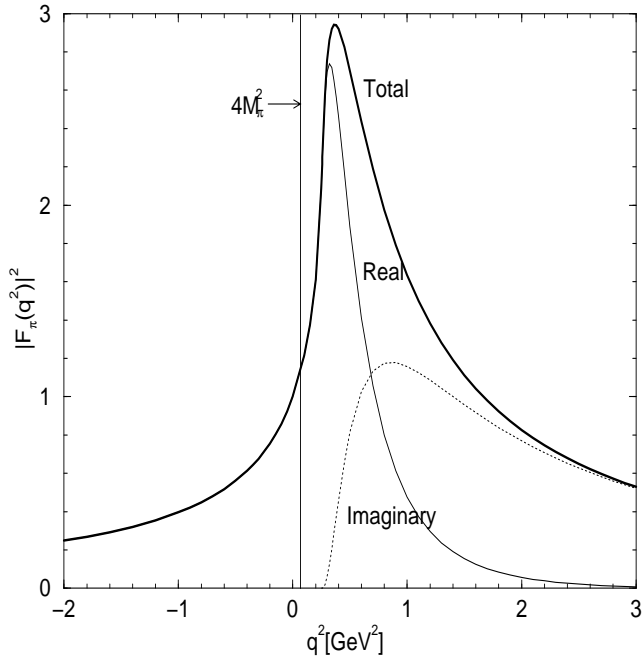


FIG. 4a. The electromagnetic form factor of the pion in $(3+1)$ dimensional scalar field theory for $-2 \leq q^2 \leq 3 \text{ GeV}^2$. The total, real, and imaginary parts of $F_\pi(q^2)$ are represented by thick solid, solid, and dotted lines, respectively.

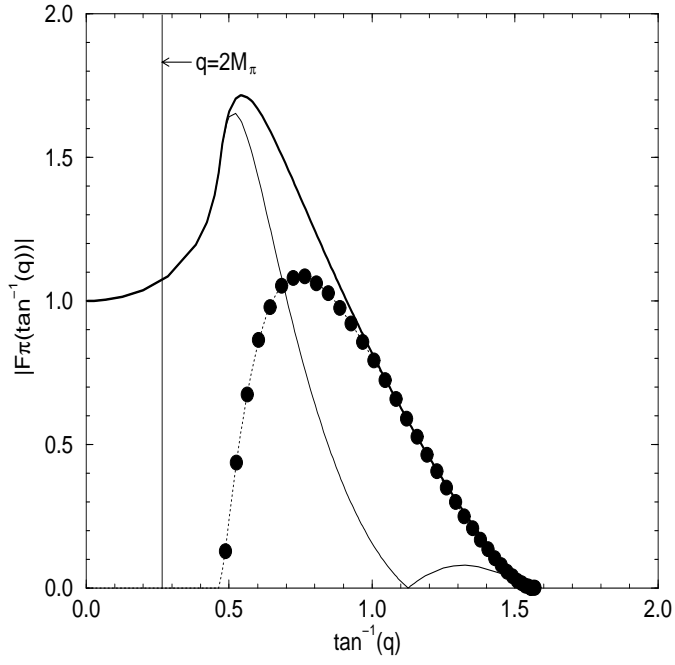


FIG .4 b. The electromagnetic form factor of the pion in $(3 + 1)$ dimensional scalar field theory for the entire timelike region compared to the dispersion relations (data of black dots) given by Eq. (25). The same line code as in Fig. 4 (a) is used.

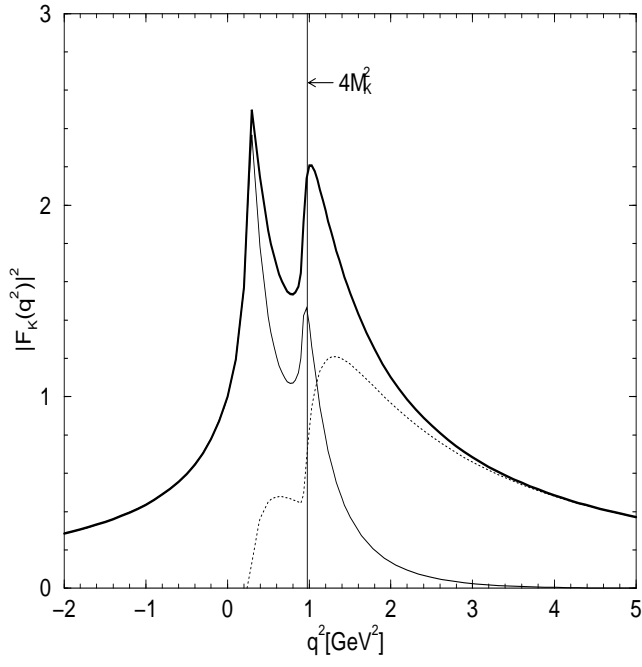


FIG. 5a. The electromagnetic form factor of the kaon in $(3+1)$ dimensional scalar field theory for $2 \leq q^2 \leq 5 \text{ GeV}^2$. The same line code as in Fig. 4 (a) is used.

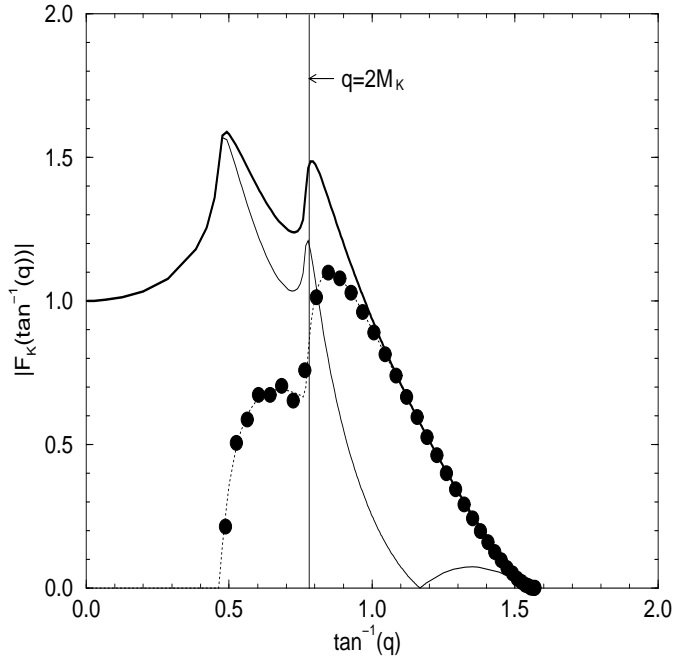


FIG .5b. The electromagnetic form factor of the kaon in $(3+1)$ dimensional scalar field theory for the entire timelike region compared to the dispersion relations (data of black dots) given by Eq. (25). The same line code as in Fig. 4(a) is used.

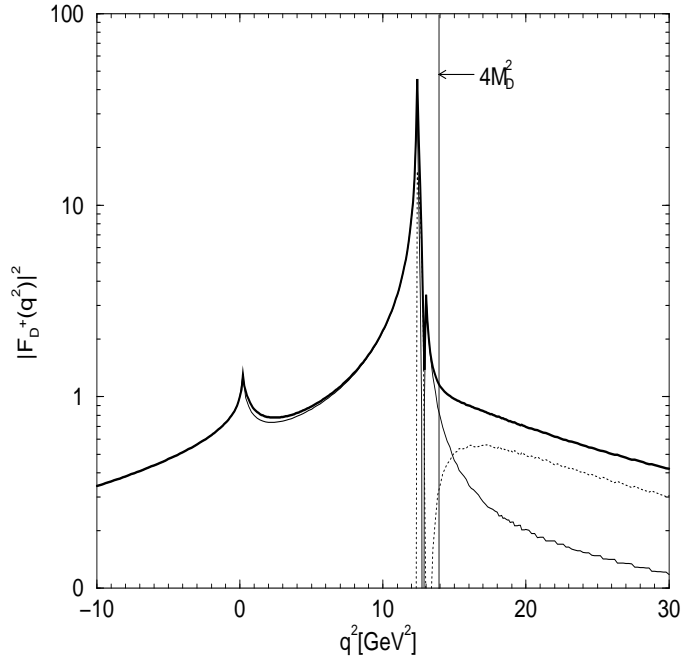


FIG .6. The electromagnetic form factor of the D meson in $(3+1)$ dimensional scalar field theory for $-10 \leq q^2 \leq 30 \text{ GeV}^2$. The same line code as in Fig. 4 (a) is used.